Towards HVDC Interoperability – Feasibility of Managing Unbalanced HVDC Operation with Offshore Converter under Islanding Control

Yaxing Ren, *Member*, *IEEE*, Md Asif Uddin Khan, Yin Chen, *Member*, *IEEE,* Mohamed A. Elgenedy, *Senior Member*, *IEEE*, Arpan Jana, and Dong Chen*, *Senior Member, IEEE*

***Abstract*— The expansion of offshore wind generation is increasing the need for interoperable and resilient HVDC transmission systems. While vendor-agnostic control architectures proposed by the Aquila project have enabled unbalanced operation in multi-terminal HVDC networks, significant challenges remain for offshore applications, particularly in hybrid bipolar configurations combining links with and without Dedicated Metallic Returns (DMRs). These challenges are amplified under N-1 contingencies and when bipolar offshore converters operate in islanded mode forming asymmetric AC networks and power flow with respect of each pole. This paper investigates the control challenges associated with connecting offshore wind farms to rigid bipolar HVDC systems under simultaneous AC asymmetry of network impedance and power infeed between poles and DC-side unbalance of the transfer network. Emphasis is placed on maintaining neutral-to-earth voltage and current within acceptable limits in the absence of a DMR, while preserving power transfer capability and peer-to-peer redundancy between parallel converters. A dedicated control strategy for bipolar offshore HVDC stations operating under islanded conditions is proposed, enabling stable unbalanced DC operation while accommodating asymmetric AC power generation and offshore network topology variations without violating AC or DC operating constraints. The proposed control strategy is validated in EMT simulations within RSCAD/RTDS environment. The tested cases include point-to-point rigid bipolar HVDC connected offshore windfarm, where comparison against library Virtual Synchronous Machine (VSM) – Voltage Source Converter (VSC) control of RSCAD, and a 5-terminal multi-purpose HVDC grid with a hybrid of full- and rigid- bipolar schemes subject to loss of pole end. All results showcase the feasibility of managing neutral voltage/current in various steady scenarios under both balanced and unbalanced HVDC operation.**

***Index Terms*— Islanding, frequency, neutral voltage control, unbalanced HVDC grid, power sharing**

I. Introduction

Towards the ambition of Great Britain in achieving its Net-ZERO ambitions, maximising the utilisation of offshore wind power [1]. HVDC interoperability has been identified as a key enabler in saving the cost of land and de-risking the supply chain. While the Aquila project [2] has demonstrated that a vendor-agnostic control architecture can ensure stable steady-state operation in an unbalanced multi-terminal HVDC network [3], such as following the loss of one pole or a section of a pole conductor in a bipolar HVDC scheme, significant uncertainties remain regarding the extension of such architectures to offshore AC-side applications.

One important application concerns the connection of offshore wind farms to bipolar HVDC systems. It is well known that a Dedicated Metallic Return (DMR), which interconnects the neutral points of a bipolar HVDC link, can enhance transmission reliability by preserving partial power transfer capability following the loss of a DC pole [3]. Such pole outages may arise, for example, from the isolation of a pole-to-earth fault. Since the DMR does not carry current during balanced operation, its primary function is to improve transfer capability under unbalanced conditions. However, when the bipolar section becomes very long, on the order of several hundred kilometres, the benefit of a DMR can become disproportionate to its cost.

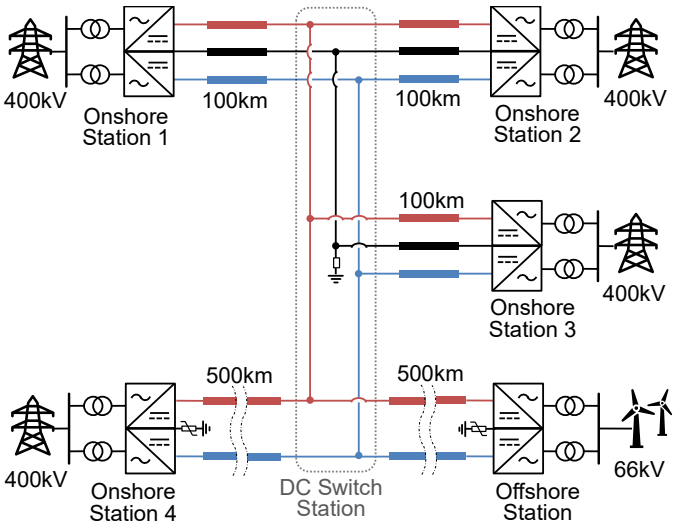

Fig. 1 Schematic diagram of five-terminal bipolar HVDC network with islanded offshore station and hybrid earthing configurations.

This imbalance frequently leads to unfavourable cost–benefit outcomes when offshore wind farms are located far from the onshore or offshore junction point. As a result, rigid bipolar HVDC configurations, i.e. bipolar schemes without a DMR, are increasingly attractive to offshore transmission owners. In other cases, networks composed of interconnected shorter DC links may justify the inclusion of DMRs, leading to hybrid HVDC grid configurations in which only selected links employ DMRs and are electrically coupled to links without DMRs. As an

* All authors are with the National HVDC Centre, UK. The paper is partially funded by the project of "Aquila Interoperability (Lite)" of SSEN-Transmission.

illustration, Fig. 1 shows a schematic of 5-terminal system where three bipolar DC connections of 100 km adopt full bipolar scheme; whereas the two links of 500 km connecting an offshore windfarm and an onshore station rigid bipolar and all links are coupled to one junction point.

Depending on system requirements, the neutral point of a rigid bipolar HVDC station may be earthed either through a surge arrester or a low-impedance path [4] for various purposes. In both cases, the neutral-to-earth voltage or current must remain close to zero, either to limit insulation requirements or to comply with regulatory constraints. Maintaining these conditions is particularly challenging in hybrid HVDC schemes that interconnect bipolar sections with and without DMRs, especially under *N-1* contingencies such as the loss of one converter pole end.

The requirement for offshore HVDC converters to connect offshore wind farms [5] further compounds these challenges. In such configurations, offshore converters must operate in islanded mode [6] and synthesize two inter-connected three-phase balanced AC voltage sources at a constant frequency.

Connecting offshore wind farms using bipolar HVDC technology further raises the technical challenges. During islanded operation, neutral current can flow into the earth and must therefore be suppressed to nearly zero. Achieving this requires the two pole converters to share the infeed power when their AC terminals are coupled, despite inherent asymmetries in the offshore AC network topology and impedance, as well as unequal power generation among turbine clusters connected to each pole. When such AC-side asymmetries coincide with DC-side imbalance, introduced by either po, the feasibility of maintaining power transfer without violating current or voltage limits on any side of the system becomes uncertain.

In addition, when the neutral point of a rigid bipolar station is earthed through a surge arrester, the neutral voltage must be maintained close to zero to prevent surge arrester degradation and to limit leakage current to earth. At the same time, achieving N-1 peer-to-peer redundancy requires parallel-connected converters to operate using identical control strategies, further constraining the control design.

To address the technological gaps above, this paper proposes a dedicated control strategy for bipolar offshore HVDC stations operating under islanded conditions. The proposed approach enables stable operation under unbalanced DC conditions while accommodating asymmetries in both AC infeed power between the two poles and the topology of the offshore AC network. Both pole converters adopt identical control structures, thereby enabling peer-to-peer redundancy.

The remainder of this paper is organized as follows. Section II presents the proposed control strategy, including the pole-level voltage space-vector and current control, as well as the station-level neutral control. Section III provides simulation results based on several case studies under different network conditions. Section IV concludes the paper and outlines directions for future work.

II. Control Strategy

This section introduces the proposed control strategy for the bipolar MMC system. The overall control architecture is shown in Fig. 2. The pole-level controller, whose detailed structure is illustrated in the figure and labelled as “Pos. Pole O/M/I-Loop Control,” comprises three hierarchical control layers: inner-loop current control, middle-loop voltage space vector (VSV) control, outer-loop differential angle control for power-sharing, parallel outer-loop common-mode frequency control for frequency regulation, station-level common-mode (secondary) frequency calculation. The “Negative Pole O/M/I-Loop Control” is identical to the “Positive Pole O/M/I-Loop Control” and is therefore not presented in detail. In addition to these, a station-level neutral-point control scheme is incorporated to regulate the neutral potential and limit undesired neutral currents through earth on the DC side.

A. Current Control Loop and Modulation Assumption

To meet the need for computationally efficient models applicable to a broad range of power system studies, this paper develops and validates a controller based on the MMC average-value model. Compared with the detailed submodule (SM) model, the average model relies on the following assumptions:

a) The switching voltages of the upper and lower arms of each phase are replaced by their averaged values in every control cycle.
b) The dynamic interactions among SMs within each arm are neglected, and the SM capacitor voltages in each arm are assumed to remain balanced.
c) The values of the upper and lower SM capacitors are identical to produce an arm-level capacitances.
d) Additional IGBTs and diodes are included to provide the necessary conduction paths for reproducing typical MMC behaviour under blocking conditions.

More detailed information regarding these assumptions and the underlying analysis of the average-value model can be found in the previously published report [7].

The current control loop is a critical inner loop that ensures reliable and efficient inverter operation. Its primary function is to protect semiconductor devices and other electrical equipment by limiting the inverter output current within permissible bounds. The current loop controller is designed as follows:

$$\begin{cases} v_{cd}^{*} = L_e \cdot H_{PI\_i}(s) \cdot (I_d^{*} - i_d) + v_d \\ v_{cq}^{*} = L_e \cdot H_{PI\_i}(s) \cdot (I_q^{*} - i_q) + v_q \end{cases} \quad (1)$$

In the current control loop, the signal i_d and i_q represent the direct (d-axis) and quadrature (q-axis) components of the converter phase current measured at the AC terminal. The reference current I_d^{*} and I_q^{*} are generated by the outer voltage control loop. The signals v_d and v_q denote the d- and q-axis components of the measured AC terminal voltage and are introduced as voltage feedforward terms to improve the dynamic performance of the converter. Filters may be applied to such feedforward voltages to supress temporary over-voltages during transients, but they are omitted in this paper for simplicity.

The outputs of the current controller, v_{cd}^{*} and v_{cq}^{*}, correspond to the d- and q-axis components of the converter voltage reference. These reference voltages are provided to the PWM modulator. The current controller is represented by the

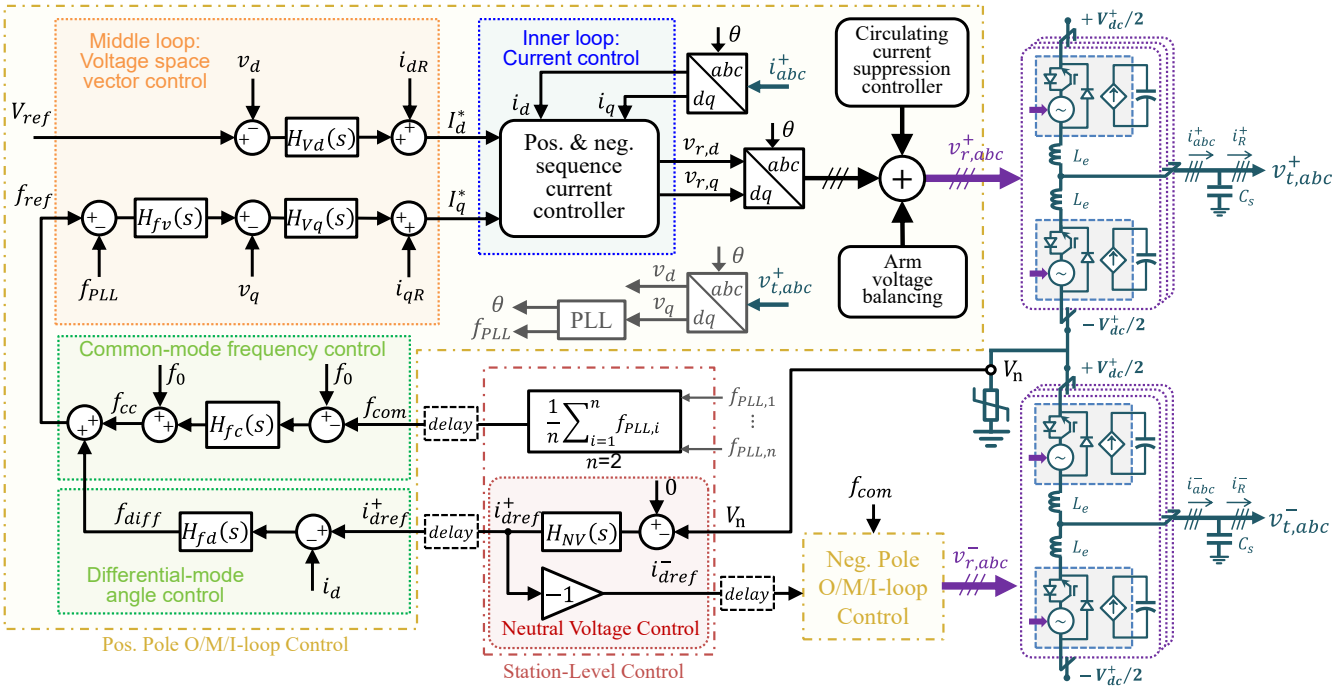

Fig. 2 Block diagram of islanding controller with neutral voltage control for bipolar MMC

transfer function $H_{PI\_i}(s)$, which is implemented as a PI regulator. The equivalent 3-phase AC voltage vector to module are then translated to abc reference frame. With the assistance of arm balancing control and circulating current suppression, the phase voltage vectors are assumed ideally modulated in every control cycle with omitted processes of capacitance balancing control and modulation process.

B. Voltage Space Vector Control Loop

The voltage control loop constitutes the middle loop. Its primary objective is to regulate the converter terminal voltage by generating appropriate current references, as expressed by:

$$\begin{cases} I_d^* = C_s \cdot H_{Vd}(s) \cdot (V_{ref} - v_d) + i_{dR} \\ I_q^* = C_s \cdot H_{Vq}(s) \cdot (v_{qref} - v_q) + i_{qR} \end{cases} \quad (2)$$

In the voltage control loop, the signals v_d and v_q correspond to the d- and q-axis components of the measured terminal AC voltage, which are identical to the voltage feedforward terms used in the current loop. The currents i_{dR} and i_{qR} represent the current flowing into the converter prior to the shunt capacitor C_s. The shunt capacitor is employed to improve voltage dynamic response by anchoring the fundamental component of the local voltage space vector. Consequently, the voltage control loop effectively regulates the current injected into the shunt capacitor. The d- and q-axis voltage controllers are represented by the transfer functions $H_{Vd}(s)$ and $H_{Vq}(s)$, respectively.

The reference signals of d- and q- components of the voltage space vector across the shunt capacitor are denoted by v_{dref} and v_{qref}. In this control design, the d-axis voltage reference v_{dref} is set to a constant value equal to V_{ref}, while the q-axis voltage reference v_{qref} is generated by the frequency control loop, as given by [8][9]:

$$v_{qref} = H_{fv}(s) \cdot (f_{ref} - f_{PLL}) \quad (3)$$

where $H_{fv}(s)$ represents the transfer function of frequency regulator, f_{ref} represents the reference value of frequency generated from the outer loop, f_{PLL} represents the measured frequency obtained from the phase-lock loop (PLL), which is typically designed to use the q-axis voltage component v_q as the feedback signal to adjust frequency, that can be designed as:

$$f_{PLL} = H_{PI}(s) \cdot v_q \quad (4)$$

C. Differential Angle Control for Power Sharing

The frequency reference is conducted as the sum of a common frequency component and a differential frequency component. The common frequency component is responsible for regulating overall system frequency drift of the AC network, whereas the differential frequency component is employed to control power sharing among converters.

$$f_{ref} = f_{cc} + f_{diff} \quad (5)$$

where f_{cc} represents the common-mode frequency command and f_{diff} represents the differential frequency command.

The differential frequency command f_{diff} is designed to regulate power distribution based on the deviation between the reference currents $i_{dref}^{+/-}$ (the superscripts "+" and "-" refers to the positive and negative poles) and the measured d-axis current i_d as:

$$f_{diff} = H_{fd}(s) \cdot (i_{dref}^{+/-} - i_d) \quad (6)$$

The AC active power can be expressed as $p = 3/2 \cdot (v_d i_d + v_q i_q)$. With PLL in operation, v_q is regulated to zero, and v_d is maintained at a constant steady-state constant V_{ref}, provided the impedance between the voltage measurements is sufficiently high to reject the differential component of measurement error. Consequently, the active power becomes

approximately proportional to i_d . The purpose of the differential frequency loop is therefore to establish a controlled relationship between converter output power and frequency. The transfer function $H_{fd}(s)$ can be designed either as a conventional static droop gain (K_{droop}), e.g. $\Delta\omega/\Delta P = -K_{droop}$, or as a first-order process, which offers similar behavior as so-called "virtual synchronous machine" [10], depending on the application requirements.

It should be noted that both $i_{dref}^{+/-}$ and I_d^* represent reference values for the d-axis current, but they serve different control objectives. The inner loop reference I_d^* is used to regulate fast internal response of AC current with high bandwidth, whereas the outer loop reference $i_{dref}^{+/-}$ operates at a lower bandwidth to regulate the power transfer between buses. The term differential frequency is used to represent the difference between the instantaneous frequencies of the two pole buses, whereas i_{dref}^{+} and i_{dref}^{-} can be assigned different reference values, and their difference effectively alters the change of power sharing between positive and negative pole.

The common-mode frequency command f_{cc} is designed to regulate the steady-state frequency of an islanded system to a predefined nominal value f_0, such as the 50 Hz nominal grid frequency used in the UK, as

$$f_{cc} = f_0 + H_{fc}(s) \cdot (f_0 - f_{com}) \tag{7}$$

where $H_{fc}(s)$ represents the transfer function of the common-mode frequency control loop, typically implemented as a PI regulator. f_{com} represents the common component of multiple local PLL output frequencies and is defined as

$$f_{com} = \frac{1}{n}\sum_{i=1}^{n} f_{PLL,i} \tag{8}$$

In a bipolar HVDC terminal, the common frequency corresponds to the average of the positive- and negative-pole PLL output frequencies, therefore, choosing $n = 2$ captures the terminal's common-mode behaviour.

If the positive- and negative-pole controllers use identical PLLs, their steady-state outputs $f_{PLL,i}$ are theoretically identical, ensuring consistent frequency regulation. However, manufacturing tolerances in clock sources and implementation discrepancies can lead to slight deviations in the measurement of time and hence PLL outputs.

Such differential frequency accumulates over time, it may result in periodic voltage angle differences when multiple islanded controllers operate in parallel, leading to undesirable circulating currents, power, or frequency oscillations, typically at a very low frequency.

By distributing the common frequency component f_{com} in (8) to all converter stations, frequency mismatches caused by clock discrepancies among local controllers can be eliminated, which is shown in Fig. 2. This concept is similar to the classical secondary control of power systems.

D. Neutral Control for Rigid Bipolar MMC

Neutral point control is implemented at the station level and is intended to eliminate undesired neutral-point current, thereby preventing current from flowing into the earth. This function is especially important in rigid bipolar converter architecture.

In rigid-bipolar converters, when the neutral-to-earth path is instead in series connection with surge arresters. Modern arresters use metal-oxide varistor (MOV) elements, which exhibit very high resistance at normal operating voltage, typically in the megaohm to hundreds-of-megaohms range, until the applied voltage approaches their conduction threshold. Due to this high equivalent impedance, the neutral-point voltage in a rigid-bipolar system becomes much more sensitive to small imbalances between the pole currents. For this reason, neutral-voltage control (NVC) is proposed, ensuring that the neutral potential is maintained within safe limits to stop current flowing into the earth and prevent unnecessary conduction of surge arrestor. The NVC can be designed as:

$$i_{dref} = H_{NV}(s) \cdot (0 - V_n) \tag{9}$$

In general terms, the impedance of neutral path can be viewed analogously to an open circuit at steady state when the control laws of (9) is implemented.

III. Case Studies

To validate the proposed control strategy, this section presents a detailed case study. An EMT model of a three-phase, three-wire islanded system is developed in RSCAD, and its configuration is shown in Fig. 3. In this setup, two 1-GW MMC stations are connected to the islanded AC system through four cross-coupled 260/66-kV transformers [11] and operate under the same islanded-control scheme. The MMC parameters are shown in Table I. The secondary sides of these transformers are connected to the busbars of two VSC-based Type-4 offshore wind farms (OWFs) via cables with differing impedances. Each OWF operates using local PQ control according to its available wind power.

TABLE I
MMC PARAMETERS

Parameters	Value & Unit
Rated power	1 GW
Rated AC voltage	260 kV
Rated DC voltage	525 kV
Number of SM	210
Arm reactance	43 mH
Arm resistance	0.0785 Ω
Equivalent arm capacitance	48.37 μF
SM capacitance	10.16 mF
AC shunt capacitance	1e-4 μF

The cross-coupled transformers serve to distribute power between OWF1 and OWF2 and to enhance redundancy in the event of offshore equipment failures. In practice, this means that if one transformer or one converter becomes unavailable, power can continue to flow through alternative paths. Functionally, the two MMCs synthesis islanded voltage sources connected to a common point through transformers. This arrangement allows evaluation of whether the two independent islanded controllers can operate without control conflict, avoid circulating power, and autonomously share power.

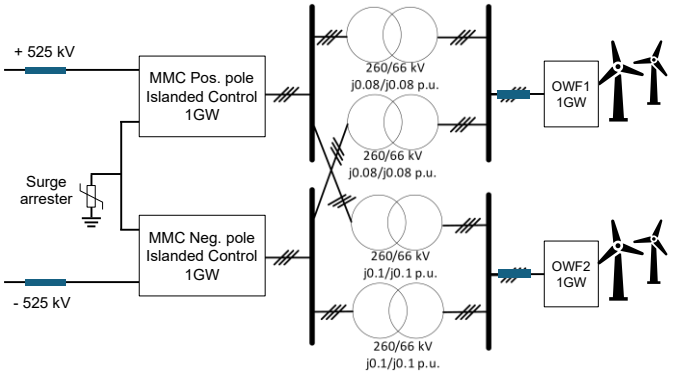

Fig. 3 Architecture of bipolar MMC for islanded OWF

To emulate realistic manufacturing tolerances, the impedances of the two cross-coupled transformer pairs are intentionally set to different values, where one pair at 0.08 p.u. and the other at 0.1 p.u. These small mismatches can cause asymmetrical distribution of AC impedances between the positive and negative poles and hence tends to cause imbalance of power sharing in between. As a result, neutral-point control becomes essential to ensure balanced operation under such conditions.

The following of this section validates the proposed control strategy under progressively more challenging operating conditions, including basic bipolar neutral-control performance, comparison with conventional VSM control, operation under asymmetric MTDC network condition, and robustness against non-ideal PLL sampling.

A. Neutral Control Validation

The effectiveness of the neutral control of a bipolar system was examined in this section. OWF1 and OWF2 each deliver 1 GW of active power to the bipolar MMC station through four cross-coupled transmission paths. Initially, the MMC station operates in rigid-bipolar mode, with the neutral point connected to earth through a surge arrester whose protection threshold is set to ±60 kV. The NVC is disabled before t = 5s and activated afterwards. The simulation results are presented in Fig. 4.

Due to impedance mismatches between the positive- and negative-pole transformers, the active power flowing into the two poles is not equal. The initial state is shown in the first 5 seconds in Fig. 4. The DC voltages of the positive and negative poles become unbalanced, as shown in Fig. 4(a). This imbalance causes the neutral-point voltage to drift and eventually reach the protection threshold of ±60 kV, as illustrated in Fig. 4(c). Once the threshold is exceeded, the surge arrester resistance drops sharply, leading to a sudden increase in the neutral current to earth, as shown in Fig. 4 (d). As the arrester conducts, the neutral-point voltage is pulled back toward zero. However, since the power imbalance between the two poles remains, the system enters a repetitive oscillatory state in which the arrester is periodically triggered.

Therefore, the oscillatory behaviour of the neutral voltage observed in Fig. 4 is not caused by any fixed-frequency resonance. Instead, it results from the system relying solely on the surge arrester for midpoint protection while the power between the two poles remains unbalanced.

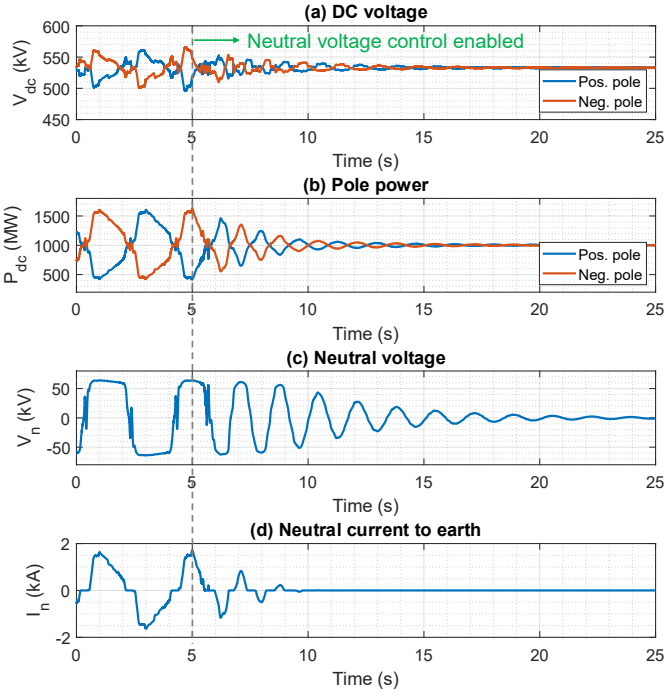

Fig. 4 Transient response of the rigid bipolar converters when the neutral voltage control is enabled. (a) DC voltage of OWF, (b) DC pole power of OWF, (c) & (d) neutral voltage and current.

The uncontrolled neutral-point voltage fluctuations also induce significant disturbances in the positive- and negative-pole DC voltages of the islanded system. A clear circulating current forms between the poles, indicating that current repeatedly flows back and forth without contributing to useful power transfer. Although the net active-power deviation for the entire station remains relatively small and does not violate the overall station power limit, each pole individually exceeds its rated power (1GW) at regular intervals, as shown in Fig.4 (b). In a practical system, this condition would be unacceptable and would normally trigger overcurrent protection, potentially leading to a forced converter shutdown.

At t = 5 s, the NVC is enabled. It demonstrates that, with the neutral control applied, the overall dynamic response of the system improves significantly. Neutral-voltage oscillations diminish and gradually converge to zero. Surge-arrester activations become both less frequent and shorter in duration. Meanwhile, the circulating current between the positive and negative poles decreases and finally stabilizes at the expected power-sharing point. These observations confirm that NVC is effective not only in balancing power distribution between the poles but also in enhancing the stability and robustness of rigid-bipolar operation.

B. Comparison with Conventional VSM-Based Control

While Section A demonstrated the dynamic behavior of rigid-bipolar operation with and without NVC, this section compares the proposed control approach with a conventional 2-level VSC based Virtual Synchronous Machine (VSM)-based strategy. For reference, this adopted VSM model is available in RSCAD FX 2.7 example section under the name of “GFM_VSG”; modifications in the example model are made to match the voltage and power level in the point-to-point model.

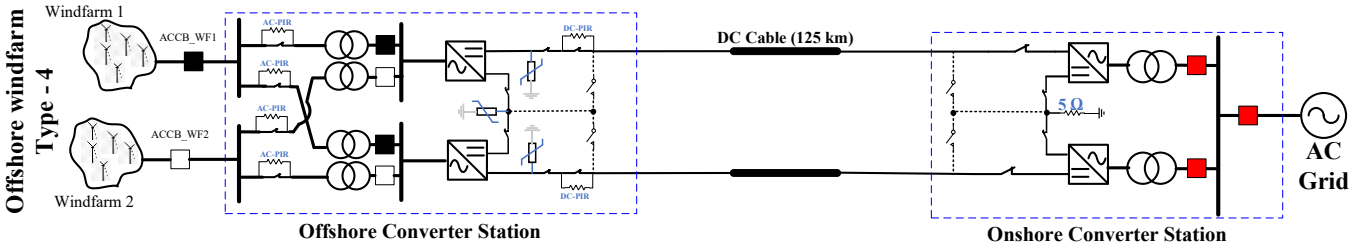

Fig. 5 Point-to-point HVDC link to interconnect windfarms to onshore focusing on offshore converter station.

However, there is no change in the control architecture of the original model.

Fig. 5 shows the point-to-point (P2P) configuration with only Windfarm 1 injecting 1 GW of active power. As discussed before, practical cross-coupled transformer arrangements inherently introduce impedance mismatches between the positive and negative poles, which can lead to unequal pole power sharing in rigid-bipolar HVDC systems. A 1% impedance mismatch is introduced between the positive- and negative-pole transformers.

Fig. 6(a) presents the response of the conventional VSM-based control under the P2P configuration. At t = 1 s, the Windfarm 1 begins generating 1 GW of power and delivers it to the converter station through the cross-coupled transformers. Under ideal conditions, the injected wind-farm power should be evenly shared between the two poles. However, the impedance asymmetry results in unequal power distribution of approximately 71.6 MW , causing a deviation of the DC neutral voltage from 0 kV to approximately -42.15 kV. Furthermore, the neutral voltage exhibits a continuous drift over time, indicating that the conventional VSM-based control lacks an inherent mechanism to regulate the neutral point under AC-side unbalanced conditions.

Although the neutral voltage rise can be temporarily constrained by installing a surge arrester at the neutral point of the offshore converter station, this approach does not provide a sustainable solution. Surge arresters are intended for transient overvoltage protection and are not designed for continuous energy dissipation. Prolonged operation under persistent neutral-point deviation may therefore lead to thermal stress, degradation of the arrester, and eventual activation of converter protection, potentially compromising system stability.

In contrast, the proposed islanded control strategy explicitly incorporates neutral-point regulation to address pole power imbalance arising from AC-side impedance asymmetries. To evaluate its effectiveness, an equivalent simulation is performed on the same offshore converter station and network configuration, with a more severe 3% impedance mismatch introduced between the positive- and negative-pole transformers. As shown in Fig. 6(b), the neutral voltage at the offshore terminal remains tightly regulated below 0.002 kV following the integration of Windfarm 1, with no observable steady-state deviation or drift. This demonstrates that the proposed control successfully suppresses DC neutral voltage imbalance under asymmetric operating conditions.

To further assess robustness, an extended real-time simulation exceeding 15 hours is conducted on the RSCAD platform. Throughout the entire simulation period, the system remains fully stable, and the neutral voltage shows no measurable variation. These results confirm that the proposed islanded control enables stable and autonomous operation of rigid-bipolar HVDC systems under practical impedance mismatches, without reliance on auxiliary hardware such as surge arresters.

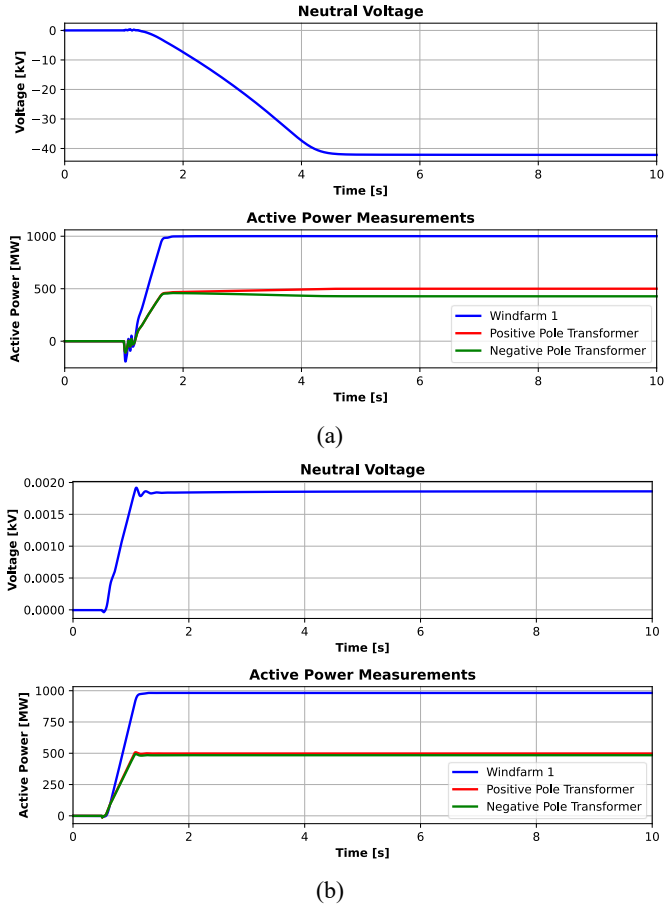

Fig. 6: Simulation results for AC side transformer impedance variation: (a) with generic VSM model, and (b) with proposed islanding control.

C. Unbalanced MTDC Network with Hybrid Earthing Scheme

In certain operating conditions, substantial asymmetry can arise between the positive and negative DC voltages, particularly in multi-terminal DC (MTDC) systems. This typically occurs when one pole of a terminal is lost, forcing power to be transferred unipolarly through the remaining healthy pole. To study this scenario, the islanded OWF system is connected to a four-terminal MTDC network, consisting of

three full-bipole terminals with DC voltage control (DVC) and one rigid-bipole terminal with power control (PC), as shown in Fig. 7. The control parameters of each terminal are shown in Table II.

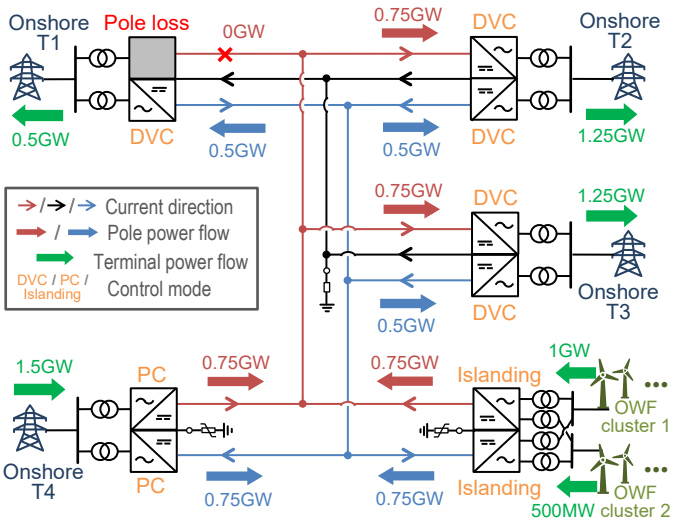

Fig. 7 Schematic diagram of a hybrid earthing multi-terminal HVDC network under asymmetric condition. (approximated power flow)

TABLE II
MAIN CONTROL PARAMETERS OF THE MTDC NETWORK

Terminal	Bipolar type	Control mode	Control	Kp	Ki
Onshore T1,2,3	Full	DVC	DC droop	0.0164	--
Onshore T4	Rigid	PC	Power	0.01	0.05
			Neutral	0.9	1
Offshore WF	Rigid	Islanding control	$H_{vd/vq}$	0.005	1e-5
			H_{fv}	0.4	--
			H_{fc}	0.9	4
			H_{fd}	0.03	--
			H_{NV}	0.1	1e-4

In the initial balanced state, the onshore terminal T4 (equipped with PC) delivers 1.5 GW of power to the DC grid. Due to varying wind conditions, OWF clusters 1 and 2 produce 1 GW and 500 MW, respectively. This power is transmitted to the DC network through the offshore HVDC converter equipped with islanding control. Onshore terminals T1, T2, and T3 (all operating with DVC) share the combined 3 GW of power from T4 and the OWFs, with each pole initially receiving 500 MW.

Fig. 8 presents the transient responses of the DC power, pole voltages, neutral-to-earth currents and voltage across all five terminals, and the AC-side states of the islanded OWF. When the positive pole of terminal T1 (a DVC terminal) is blocked at t = 5 s, its incoming power instantaneously drops to zero, as shown in Fig. 8(a), leading to a rapid rise in its positive pole voltage to approximately 570 kV, as shown in Fig. 8(f). Consequently, the remaining terminals experience imbalanced power distribution, e.g. the received power on the positive poles of T2 and T3 increases from 500 MW to 750 MW.

Under such sustained voltage asymmetry, neutral-point control becomes essential. For the rigid-bipole terminal T4, overvoltage must be avoided following the pole-loss transient. As a result, its sending power momentarily decreases from 750 MW to approximately 650 MW to maintain DC voltage, and then gradually returns to 750 MW once the DC voltage settles. Since T4 is a rigid bipole and prohibits neutral current flow, the reduction in positive-pole current forces a synchronous reduction in negative-pole current to avoid pole-current imbalance as in Fig. 8(d). In contrast, the power reduction at the OWF terminal is not feasible due to fixed wind generation and slow mechanical dynamics, and thus its output power does not drop significantly.

Fig. 8(k)–(o) show the resulting neutral-current behavior at each terminal. Following the blocking of T1's positive pole, T1's neutral current immediately shifts from 0 to –0.9 kA, forming the return path to the negative pole. At the meantime, terminals T2 and T3 share the compensating neutral-current rise, each increasing from 0 to approximately 0.45 kA. As both T4 and the OWF terminal operate as rigid bipoles, neutral-to-earth current is suppressed, and no significant increase is observed at these terminals. The highest neutral voltage among all terminals is approximately 24 kV, occurring at the two rigid bipolar terminals, T4 and OWF. As shown in Fig. 8(p), this confirms that the neutral voltages at all terminals remain below 5% of the rated voltage and decays to the range within 2 kV in 30 seconds. For surge arrestor of protective voltage at 50 kV, such performance should stay within the range of continous operation.

Fig. 8(q)–(t) depict the OWF AC-side transient responses. During the pole loss at T1, the OWF AC bus voltage and frequency experience noticeable but acceptable transient deviations, remaining close to 66 kV and 50 Hz, respectively. Although OWF clusters 1 and 2 generate different wind power levels, the cross-coupled transformers and islanding control strategy redistribute power such that the DC-side injection remains balanced.

These results demonstrate that the proposed neutral-control strategy remains effective under both transient and steady-state voltage imbalance. The method provides robust fault-ride-through capability and ensures stable long-term operation of the MTDC-connected OWF system.

D. Robustness of Using Common-Mode Frequency against Asynchronous Clocks of PLLs

The preceding case studies verified the controller's stability and robustness under a variety of operating-point transitions and network disturbances. However, all previous assessments assumed ideal control signals.

To assess controller robustness under this non-ideal measurement condition, a final test is conducted using a deliberately mismatched integrator sampling time. To isolate and highlight the impact of the sampling-time mismatch on the AC side, this test was performed on the islanded OWF terminal using an ideal DC source rather than the MTDC system. As shown in the three left-hand plots in Fig. 9, the system initially

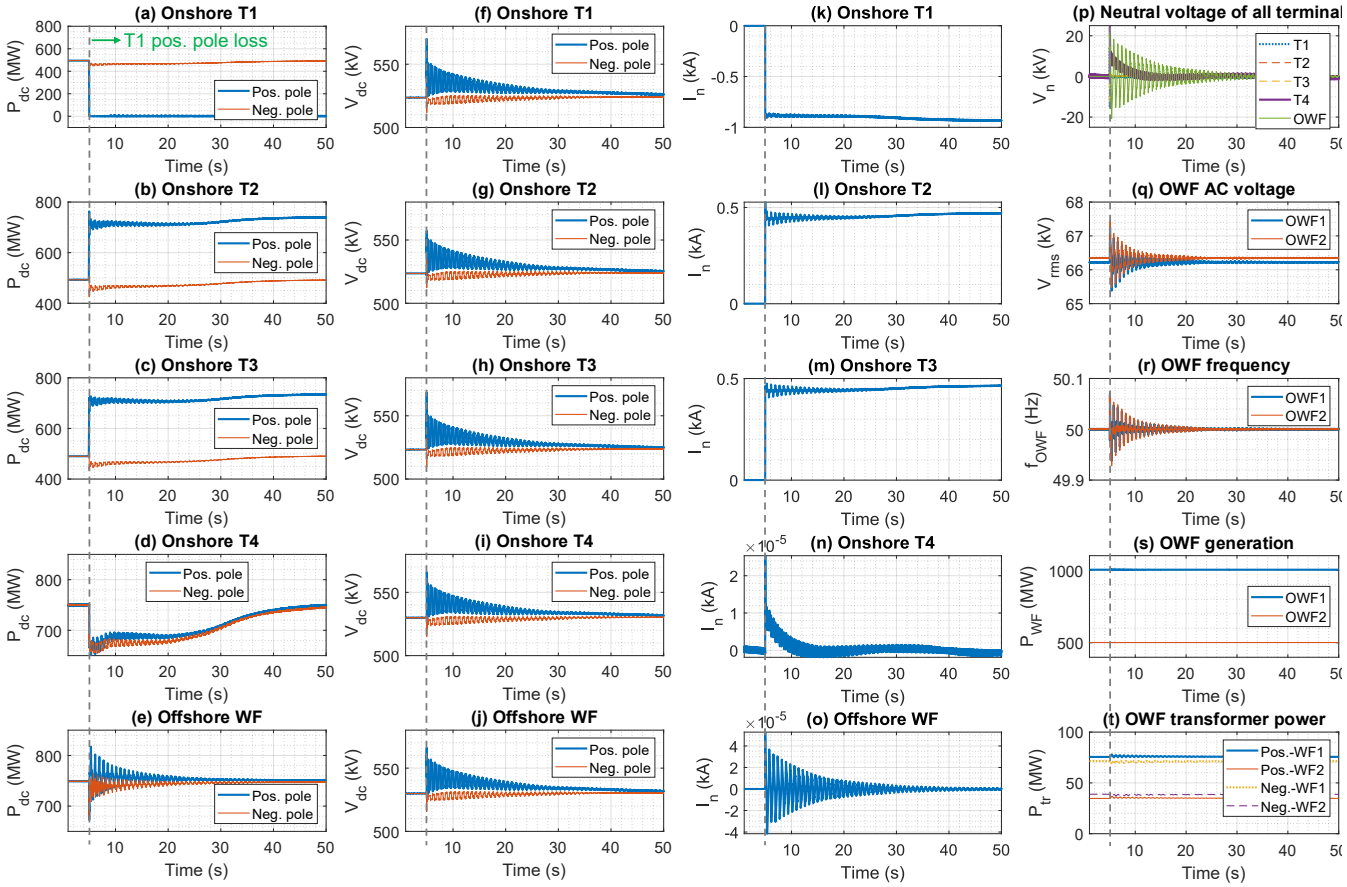

Fig. 8 Transient response of 5-terminal DC network under unbalanced conditions when a pole loss fault occurs. (a)-(e) DC pole power flow of each terminal, (f)-(j) DC pole voltage of each terminal, (k)-(o) neutral current flow at each terminal, (p) neutral voltage of all terminals, (q)-(t) AC bus voltage, frequency, power generation and transformer power delivery of the islanding controlled OWF station.

operates in islanded balanced mode, with the positive and negative poles each supplying 750 MW. In this operating state, both poles rely on their local PLL frequency f_{PLL} rather than the common-mode reference f_{com}. When the PLL sampling time for both poles are identical, their voltage and power remain balanced.

At t = 2 s, a small 0.1% increase in the PLL integrator sampling time at the positive pole introduces a steady drift in the relative angle of the voltage space vector between the poles. This angular deviation alters the power sharing, causing the power difference between the poles. The resulting imbalance manifests as neutral-voltage drift and increased neutral current to earth, even when the same neutral-point controller is in operation.

Note: the 50 kV neutral voltage in Fig. 9 is an illustrative consequence subject to absence of common-mode frequency regulation, which may trigger the clamping effect of the surge arrester.

When the common frequency loop switches from local PLL-based reference f_{PLL} to the centralised reference f_{com} at t = 90 s, the angular difference collapses rapidly, and the neutral-point voltage returns to zero, as shown in the three plots on the right of Fig. 9. Notably, even though the underlying PLL integrator mismatch still exists, it no longer affects controller performance or system stability.

These results confirm that adopting a shared frequency reference effectively removes the long-term phase-drift mechanism, ensuring robust operation even in the presence of non-ideal timing conditions.

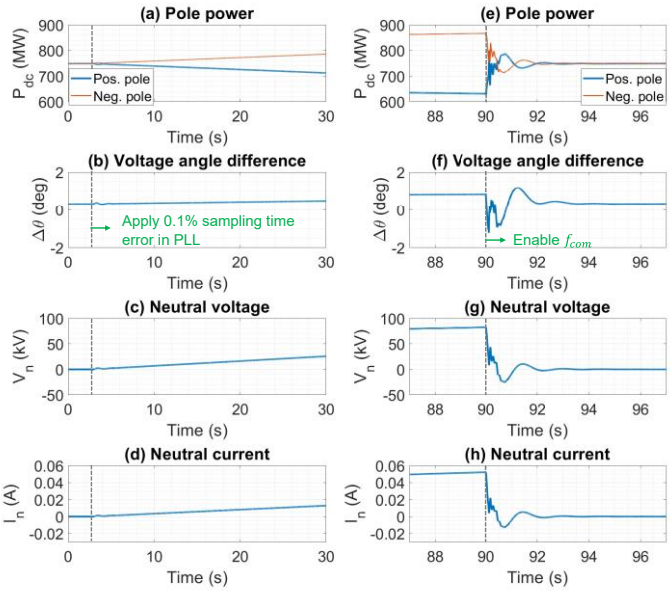

Fig. 9 Using the centralised common frequency to mitigate frequency oscillations during PLL clock mismatch.

IV. Conclusion and Future Work

This paper has demonstrated that simultaneous regulations of both frequency of offshore island and neutral-point DC voltage is achievable in rigid bipolar HVDC-connected offshore wind farms. By applying a local feedback controller to the neutral-point voltage across the earthing surge arrester at a rigid bipolar terminal, power sharing between the positive and negative poles can be actively shaped, enabling continuous suppression of neutral-point voltage and hence the leakage current flowing through the surge arrestor alike. This capability is preserved even under unbalanced operating conditions, such as the loss of one pole in the connected bipolar HVDC network.

In parallel, frequency regulation based on feedback control allows effective management of power sharing within the AC island, despite asymmetries in AC network impedance and unequal power distribution between poles. To achieve tight frequency regulation with zero steady-state error, however, limited data exchange between the poles becomes necessary. Such communication prevents accumulation of frequency-measurement discrepancies and can be implemented through a relatively slow, centralised coordination mechanism.

The neutral-point voltage regulation approach presented here, designed for high-impedance surge-arrester earthing, and its counterpart, neutral-current regulation for low-impedance earthing or fully floating full-bipolar configurations, are applicable to both offshore and onshore bipolar converter stations.

Transitions between these earthing schemes to manage various contingencies, along with the associated control adaptations, are expected to be feasible within acceptable operational boundaries. Detailed investigation of these transition dynamics and the development of coordinated control strategies are reserved for future report.

V. References

[1] Department for Energy Security & Net Zero, Offshore Wind Net Zero Investment Roadmap. London, U.K.: UK Government, Mar. 2023. [Online].Available: https://www.gov.uk/government/publications/offshore-wind-net-zero-investment-roadmap. Accessed: Mar. 2, 2026.

[2] D. Chen, P. Phurappa, B. Marshall, A. Scott, and C. Henderson, “Towards HVDC interoperability—Vendor agnostic control architecture and quantifying domain of operating point,” IET Generation, Transmission & Distribution, vol. 19, no. 1, article e13298, Mar. 2025, doi: 10.1049/gtd2.13298.

[3] D. Chen, P. Phurappa, B. Marshall, M. W. Ahmad, and C. Henderson, “Towards HVDC Interoperability – Neutral Current Control for Multiple Terminals,” EasyChair Preprint no. 13292, May 2024.

[4] M. K. Bucher and C. M. Franck, "Comparison of fault currents in multiterminal HVDC grids with different grounding schemes," 2014 IEEE PES General Meeting | Conference & Exposition, National Harbor, MD, USA, 2014, pp. 1-5, doi: 10.1109/PESGM.2014.6938990.

[5] E. Spahic and G. Balzer, "Offshore wind farms - VSC-based HVDC connection," 2005 IEEE Russia Power Tech, St. Petersburg, Russia, 2005, pp. 1-6, doi: 10.1109/PTC.2005.4524445.

[6] H. Suwa et al., "PSCAD/EMTDC and RTDS Simulation Analysis of Multivendor Multi-terminal HVDC System Connected to Offshore Windfarms," 2018 International Power Electronics Conference (IPEC-Niigata 2018 -ECCE Asia), Niigata, Japan, 2018, pp. 1997-2002, doi: 10.23919/IPEC.2018.8508011.

[7] University of Strathclyde & The National HVDC Centre, “Development and Validation of Offline and Real-time User-defined Models of Alternative MMC Configurations,” Technical Report USTRATH-HVDC Centre-P1-004, Issue 4, pp. 1–41, Sep. 26, 2018. [Online] Available: https://www.hvdccentre.com/wp-content/uploads/2019/12/The-National-HVDC-Center-Project-Report-I-MMC-Modelling.pdf

[8] Xiaozuo Huang, Dong Chen and Lie Xu, “Microgrid design using folded P-f droop and new grid interface unit to minimize the need for communication”, International Journal of Electrical Power & Energy Systems, Volume 130, 2021, 106949, ISSN 0142-0615, https://doi.org/10.1016/j.ijepes.2021.106949.

[9] Dong Chen . PLL-Based Control Strategy for Interconnecting Multiple VSCs under Islanded Control. TechRxiv. September 19, 2025.

[10] Q. -C. Zhong and G. Weiss, "Synchronverters: Inverters That Mimic Synchronous Generators," in IEEE Transactions on Industrial Electronics, vol. 58, no. 4, pp. 1259-1267, April 2011, doi: 10.1109/TIE.2010.2048839.

[11] A. Alefragkis and S. Kabul, “Next Generation Offshore Grid Connection Systems: TenneT’s 2 GW Standard,” ELECTRA, no. 321, Apr. 2022.